Science Advances

AAAS

advances.sciencemag.org/cgi/content/full/3/11/eaao5173/DC1

Supplementary Materials for

Two-dimensional limit of crystalline order in perovskite membrane films

Seung Sae Hong, Jung Ho Yu, Di Lu, Ann F. Marshall, Yasuyuki Hikita, Yi Cui, Harold Y. Hwang

Published 17 November 2017, *Sci. Adv.* **3**, eaao5173 (2017)
DOI: 10.1126/sciadv.aao5173

This PDF file includes:

- fig. S1. Growth of $SrTiO_3/Sr_3Al_2O_6$ films.
- fig. S2. Transfer of $SrTiO_3$ membranes.
- fig. S3. Chemical stability of $SrTiO_3$ films.
- fig. S4. Strain test using AFM force spectroscopy.
- fig. S5. In situ heating experiment in TEM.
- Control experiments
- Continuum elastic theory and atomic potential model
- References (*34*, *35*)

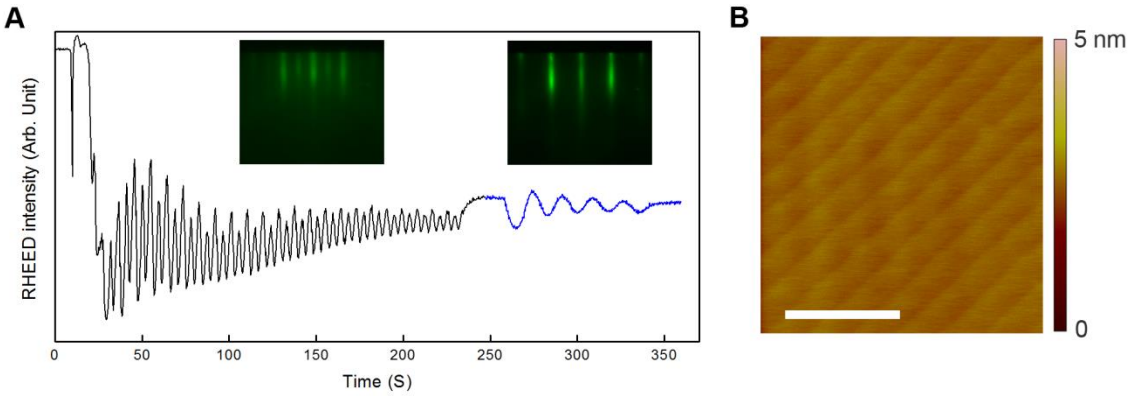

fig. S1. Growth of $SrTiO_3/Sr_3Al_2O_6$ films. (**A**) RHEED oscillations of $Sr_3Al_2O_6$ (black) and $SrTiO_3$ (blue) growth. Inset: RHEED patterns after $Sr_3Al_2O_6$ layer growth (left) and $SrTiO_3$ layer growth (right). (**B**) AFM image of $Sr_3Al_2O_6$ 20 nm / $SrTiO_3$ 4 nm deposition, showing an atomically smooth surface with step and terrace surface with perovskite unit cell steps. The scale bar indicates 2 μm.

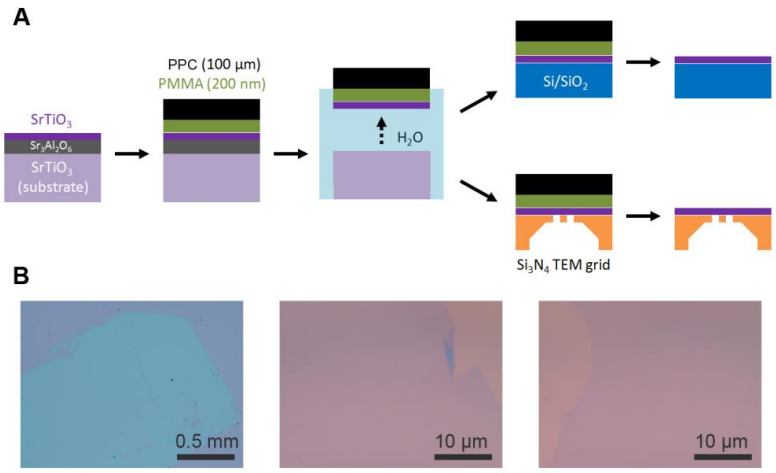

fig. S2. Transfer of $SrTiO_3$ membranes. (**A**) Schematic of $SrTiO_3$ layer release and transfer. During the sacrificial layer dissolution in water, the thick polymer layer functions as a mechanical support. (**B**) Optical images of transferred $SrTiO_3$ layers on oxidized Si (SiO_2 300 nm) substrates, for 6 u.c. (left and center), and 4 u.c. (right). The measured AFM height profile well matches the thickness monitored by RHEED oscillations.

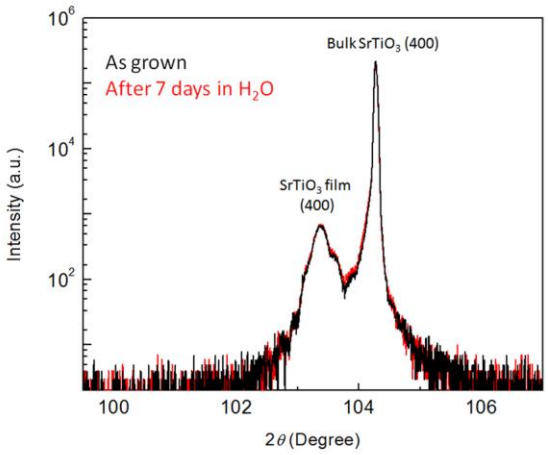

fig. S3. Chemical stability of $SrTiO_3$ films. XRD pattern around $SrTiO_3$ (400) of a 100 nm thick $SrTiO_3$ film grown on a bulk $SrTiO_3$ (100) substrate, before (black) and after (red) exposure to room temperature deionized water for a week. The $SrTiO_3$ film was grown slightly off-stoichiometry intentionally, in order to distinguish the film peak from the bulk substrate peak. The two film XRD peaks before and after exactly overlap each other.

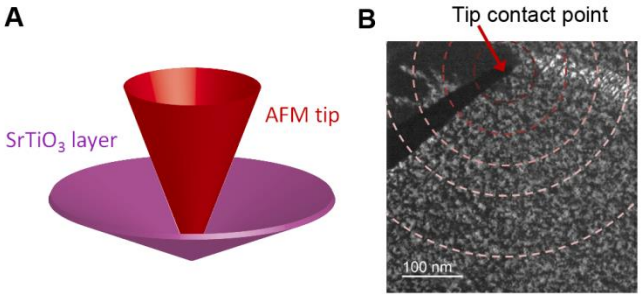

fig. S4. Strain test using AFM force spectroscopy. (**A**) Schematic of the AFM force spectroscopy. An AFM tip (ACTA tip with force constant 40 N/m) was used to apply tensile strain on a $SrTiO_3$ membrane suspended on a 2 μm hole, until the membrane fractured. (**B**) A DF-TEM image of a 4 u.c. $SrTiO_3$ membrane after the fracture by AFM. The concentric circles indicate the same distance from the fracture point. The black area is a crack and bright and dark areas are tilted from the reference plane.

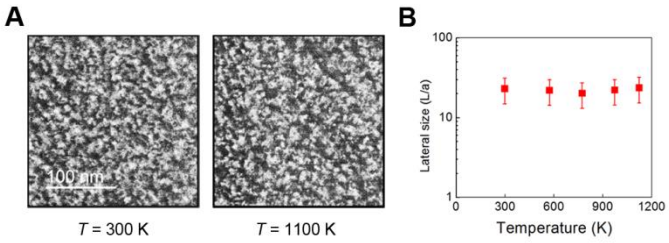

fig. S5. In situ heating experiment in TEM. (**A**) DF-TEM images of a 4 u.c. $SrTiO_3$ membrane at two different temperatures. (**B**) Crystalline domain size of a 4 u.c. $SrTiO_3$ membrane *vs* temperature.

Control experiments

We carefully examined possible extrinsic factors affecting the crystal structure of the $SrTiO_3$ membranes. Electron beam damage, mechanical/thermal energies, and chemical reaction were considered and tested by diverse material characterization methods such as TEM, X-ray diffraction (XRD), RHEED, and AFM. The results exclude these factors as origins of the observed structural change, confirming the wide stability window of $SrTiO_3$. These control experiments are described in detail below.

Chemical reaction and the surface crystalline phase – in order to verify the chemical stability of $SrTiO_3$ crystals in water and organic solvents, we studied both bulk and surface crystalline structure of $SrTiO_3$ films and membranes. One of the possible chemical reactions is Sr leaching from the $SrTiO_3$ crystals. We first used XRD to test chemical stability of $SrTiO_3$ films in water. XRD patterns of a 100 nm-thick $SrTiO_3$ film on a single crystalline $SrTiO_3$ (001) substrate, before and after the immersion in room temperature deionized water (7 days), were compared (fig. S3). The identical XRD patterns confirmed the stability of $SrTiO_3$ during this process.

In addition, we also performed surface characterization of $SrTiO_3$ films by monitoring *ex situ* RHEED after each step (Fig. 3). All $SrTiO_3$ films grown on $Sr_3Al_2O_6$ / $SrTiO_3$ substrate were single crystalline regardless of their thickness. The RHEED patterns were all identical from 1 u.c., suggesting that the RHEED pattern is a very effective probe of the topmost surface structure. The films were also tested under the exposure to all steps used in the membrane fabrication. After long and sequential exposure to water, polymer (PMMA), and organic solvents (acetone and isopropyl alcohol) mimicking the actual fabrication steps, $SrTiO_3$ films (2, 4, 8 u.c. thickness) grown on $Sr_3Al_2O_6$ / $SrTiO_3$ substrate maintained their single crystalline surface, confirmed by the identical RHEED patterns as the as-grown films (Fig. 3, middle). By contrast, the transferred $SrTiO_3$ membranes showed a drastic change in RHEED, consistent with the TEM results (Fig. 2). The 2 u.c. thick $SrTiO_3$ membrane showed no detectable RHEED pattern, and the 4 u.c. thick membrane had a very weak RHEED spot, while the 8 u.c. thick membrane shows almost an identical pattern as the film before lift-off (Fig. 3, bottom).

Mechanical strain – we have tested both compressive and tensile strain applied on $SrTiO_3$. We applied large tensile strain in the membranes using an atomic force

microscopy (AFM) tip with enough force to break them (fig. S4). The membrane thus experienced a tensile strain with an amplitude proportional to 1/(distance from the tip contact point). Based on the AFM force spectroscopy model (circular membrane under a spherical indenter) (*34*), we estimated the maximum strain at the AFM tip radius (10 nm) to be 10%. From that, the 1st, 2nd, 3rd, and 4th circles in fig. S4B corresponds to iso-stain lines of 2%, 1%, 0.67%, and 0.5% respectively. From the DF-TEM mapping, we do not find any change as a function of the tensile strain magnitude in this range of strain. A separate measurement of 1) thermal expansion coefficient of the polymer support and 2) tension in membranes estimated by the AFM force spectroscopy estimates the actual strain during the transfer is at most 0.1 – 0.2%, much smaller than the strain in our control experiment by the AFM force applied.

The maximum compressive stress during the fabrication process is about 8 MPa applied by critical point drying (CPD) using CO_2 superfluid transition. We prepared a $SrTiO_3$ film grown on a $SrTiO_3$ substrate and confirmed that its RHEED patterns before and after the CPD process are identically single crystalline. We also found no difference between membranes transferred by two different transfer methods (with and without the high-pressure step by CPD).

Thermal energy – with an *in situ* TEM heating holder, we monitored the DF-TEM images of a 4 u.c. membrane at different temperatures. Within the temperature range from 300 K to 1150 K, we did not see any change in the crystalline coherence length in spite of the ~400 % increase of the thermal energy k_BT (fig. S5), excluding a melting temperature change in smaller crystalline systems (*27*) and other thermally driven phase transitions.

Beam-induced melting – we observe beam-induced damage of the suspended membranes when we use an acceleration voltage of 300 kV and a very small field of view. Either using 80 kV or taking images at large field of view solved this issue, by confirming that the crystalline domains were not changing with a long exposure time. In addition, to reduce any potential effect by beam exposure, we first adjusted the beam focus at the nearest suspended membrane and moved to the target membrane to minimize the focusing time in measurements.

Continuum elastic theory and atomic potential model

Born-Lande model calculation of the critical thickness in 2D membranes - the critical thickness d_{BKT} was calculated based on two assumptions: the dislocation energy in 2D membranes follows continuum elastic theory, and the fluctuation energy is from the out-of-plane bonding energy generated during the membrane release process. We first set an atomic potential model of an arbitrary bonding nature, for which the potential $U(r)$ at atomic distance r is described by repulsive and attractive interaction terms

$$U(r) = C_1[\frac{r_0}{r}]^{\alpha} - C_2[\frac{r_0}{r}]^{\beta} \quad (1)$$

where C_1 and C_2 are positive constants defined by E the potential well depth, r_0 the equilibrium position, and α and β are the powers of repulsive and attractive terms respectively. Two constants C_1 and C_2 are deduced by the boundary condition at $r = r_0$

$$U(r_0) = -E,\ \frac{\partial U}{\partial r}_{r=r_0} = 0 \tag{2}$$

where α and β depend on the bonding nature and the crystal structure. For the calculation of ionic crystals, we use the Born-Lande Equation (*29*). The attractive interaction is the Coulomb potential ($\beta = 1$), while the repulsive potential depends on the chemical composition. The Born exponent (α) is typically between 5 and 12, determined by the ion configuration.

The Born exponent α of a specific ionic crystal is calculated from the average of individual atoms in the compound (*29*). For example, $SrTiO_3$ contains five atoms in a single unit cell. The electronic configurations of Sr^{2+}, Ti^{4+}, and O^{2-} are Kr ($\alpha = 10$), Ar ($\alpha = 9$), and Ne ($\alpha = 7$) respectively. Therefore the averaged α for $SrTiO_3$ is (10+9+7+7+7)/5 =8.

Elastic properties such as the 3D Young's modulus (Y) can be directly calculated from the atomic potential term by definition

$$Y(E, \alpha, \beta) = \frac{1}{r_0}\frac{\partial^2 U}{\partial r^2}_{r=r_0} \tag{3}$$

BKT theory *(3, 5, 6, 35)* anticipates the critical fluctuation energy ($k_B T_{BKT}$) to be of order of the 2D dislocation energy (~ Ka^2, K: 2D Young's modulus, a: lattice constant), with a prefactor of $1/16\pi$. In this experiment, the fluctuation energy is the out-of-plane bonding energy ($E_\perp$). In contrast, the 2D dislocation energy only counts the in-plane bonding energy ($E_{/\!/}$), thus K is $Y(E = E_{/\!/})d$. The relation between bonding energies and critical thickness (d_{BKT}) is

$$E_\perp = \frac{1}{16\pi} Y_{E=E_\parallel}\, d_{BKT}\, a^2 \tag{4}$$

where Y is calculated from Equation 3. Equation 4 is identical to Equation 1 in the main text.